

# On the origin of the Almahata-Sitta meteorite and 2008 TC<sub>3</sub> asteroid

Julie Gayon-Markt<sup>1\*</sup>, Marco Delbo<sup>1</sup>, Alessandro Morbidelli<sup>1</sup>, Simone Marchi<sup>1,2</sup>

<sup>1</sup>Laboratoire Lagrange UMR 7293, Université Nice Sophia-Antipolis, CNRS, Observatoire de la Côte d'Azur, B.P. 4229, 06304 Nice Cedex 4, France.

<sup>2</sup>NASA Lunar Science Institute, Center for Lunar Origin and Evolution, Southwest Research Institute, 1050 Walnut St, Suite 300, Boulder, CO 80302, USA.

Accepted 2012 May 1.

## ABSTRACT

Asteroid 2008 TC<sub>3</sub> was a Near Earth Asteroid that impacted the Earth on 2008 October 7. Meteorites were produced by the break-up of 2008 TC<sub>3</sub> in the high atmosphere and at present, about 600 meteorites - called Almahata Sitta - coming from 2008 TC<sub>3</sub> have been recovered. A mineralogical study of Almahata Sitta fragments shows that the asteroid 2008 TC<sub>3</sub> was made of meteorites of different types (ureilites, H, L, and E chondrites). Understanding the origin of this body and how it was put together remain a challenge. Here we perform a detailed spectroscopical and dynamical investigation to show that the most likely source region of 2008 TC<sub>3</sub> is in the inner Main Belt at low inclination ( $i < 8^\circ$ ). We show that asteroids with spectroscopic classes that can be associated with the different meteorite types of Almahata Sitta are present in the region of the Main Belt that includes the Nysa-Polana family and objects of the Background at low inclination. Searching for a possible scenario of formation for 2008 TC<sub>3</sub>, we show that there is little chance that 2008 TC<sub>3</sub> was formed by low velocity collisions between asteroids of different mineralogies, in the current asteroid belt. It seems more likely that the heterogeneous composition of 2008 TC<sub>3</sub> was inherited from a time when the asteroid belt was in a different dynamical state, most likely in the very early Solar System. Because ureilites are fragments of a large, thermally metamorphosed asteroid, this suggests that the phases of collisional erosion (the break-up of the ureilite parent-body) and collisional accretion (the formation of the parent body of 2008 TC<sub>3</sub>) overlapped for some time in the primordial asteroid belt.

**Key words:** techniques: spectroscopic – catalogues – meteorites, meteors, meteoroids – minor planets, asteroids: individual: 2008 TC<sub>3</sub>

## 1 INTRODUCTION

Meteorites are a partial sample of asteroids that survive the passage through the Earth's atmosphere. The identification of the source regions of the different type of meteorites is essential to be able to link the mineralogical properties of meteorites to the parent asteroids and, consequently, to address the mineralogical evolution in the asteroid belt. However, this is not an easy task and only some of these links could be established: for instance, the group of howardites, eucrites, and diogenites (HEDs) meteorites are thought to come from the Vesta family of asteroids (e.g. Binzel & Xu 1993); more speculatively, L ordinary chondrites could come from the Gefion family (Nesvorný et al. 2009), while asteroids of the the Flora family bear spectral similarities with the LL chondrites (Vernazza et al. 2008). However, the parent bodies of most meteorite types, if still intact, are unknown.

The discovery and spectroscopic observation of the

near-Earth asteroid (NEA) 2008 TC<sub>3</sub> (henceforth TC<sub>3</sub>) 20 hours before it impacted the Earth's high atmosphere, and the subsequent recovery of meteorites (called Almahata Sitta) – clearly coming from this body – was a major result in this respect (Jenniskens et al. 2009; Shaddad et al. 2010). It allowed a direct link between an asteroid and meteorites to be established for the first time: the asteroid was classified as belonging to the spectroscopic F-class (in the Tholen classification, Tholen 1984) or B-class (in the Bus classification, Bus & Binzel 2002) on the basis of the flat shape of its reflectance spectrum in the region between 500 and 1000 nm. Moreover, among the 47 meteorites initially recovered, it was observed that the visible spectrum of the fragment #7 matches the telescopic spectrum of TC<sub>3</sub> obtained before the impact with the Earth's atmosphere (Jenniskens et al. 2009). Fragment #7 is an achondrite polymict ureilite (Jenniskens et al. 2009). Ureilites are in a group of achondritic meteorites that exhibit both primitive and evolved characteristics (Cloutis et al. 2010): in particular, they are characterized by olivine and pyroxene-rich clasts among carbaceous material (mainly graphite); fine-

\* E-mail: julie.gayon@oca.eu

grained graphite is also present, which lower the albedo of the meteorites (about 10-12%; Hiroi et al. 2010). Ureilites were initially thought to derive from *S*-class asteroids (see for instance Gaffey et al. 1993). However, because of its spectral properties, Jenniskens et al. (2009) propose a link with *B*-class asteroids according to the Bus classification or *F*-class in the Tholen classification. This is more plausible than a link with *S*-class asteroids, given the low albedos of ureilite meteorites, consistent with *B* or *F*-class asteroids but not with the *S*-class.

It is worth to note that the *F*-class can be distinguished from the *B*-class from a much weaker UV drop-off in the spectra of the former compared to the latter and also because *B*-class asteroids show a moderately higher average albedo than *F*-class bodies. However, in the Bus classification these two classes are merged in a unique class (the *B*-class). This is because the Bus & Binzel (2002) spectral classification is based on spectra acquired with CCD spectrographs, which – in general – do not observe far enough in the UV to observe the above-mentioned drop-off feature. We will refer in this work to *B*-class asteroids including both Tholen *B*- and *F*-classes, and Bus *B*-class.

Interestingly, mineralogical studies of Almahata Sitta show that, among the  $\sim 600$  fragments recovered (Shaddad et al. 2010), about 70 – 80% are ureilites, while the remaining 20 – 30% are enstatite chondrites, H and L ordinary chondrites. More specifically, Bischoff et al. (2010) show that, among a subsample of 40 deeply studied meteorites from Almahata Sitta, 23 fragments are achondritic ureilites and 17 have chondritic litologies with 14 of them corresponding to enstatite chondrites, 2 to H ordinary chondrites and 1 to a new type of chondrite (see Horstmann et al. 2010 for more details). Although small clasts of different types are quite common in brecciated meteorites (see Meibom & Clark 1999, for a review) and carbaceous material is found in some HED meteorites, it is the first time that meteorites of very different mineralogies (i.e. primitive fragments with achondritic polymict ureilites and evolved ones such as ordinary chondrites or enstatite chondrites) are associated to the same fall. This led to make the hypothesis that TC<sub>3</sub> was an asteroid made of blocks of different mineralogies, held together very loosely (given the explosion of the body at the anomalously high altitude; Jenniskens et al. 2009; Bischoff et al. 2010; Shaddad et al. 2010).

Tracing back TC<sub>3</sub> to its source region in the asteroid Main Belt would allow us to understand the origin of the Almahata Sitta meteorites and how TC<sub>3</sub> was put together by loosely assembling meteorites of different mineralogies. Establishing this link would also be fundamental to shed light on the source region of ureilites, that albeit rare, are the forth major class of primitive meteorites recovered on Earth after the CV, CI and CO carbonaceous chondrites.

In their attempt to find the source region of TC<sub>3</sub> and Almahata Sitta, Jenniskens et al. (2010) selected all *B*-class asteroids, according to the Bus classification, and objects of the Tholen *F* and *B* classes and searched for spectra similarities with TC<sub>3</sub> and Almahata Sitta. As a result of their study, they showed spectral similarities between TC<sub>3</sub> and ungrouped asteroids as well as several dynamical asteroid groups (or families) as possible origins for the TC<sub>3</sub> asteroid, namely Polana (2.4 AU, 3°), Hoffmeister (2.8 AU, 4.5°), Pallas (2.8 AU, 33°), Themis (3.15 AU, 1.5°), and

Theobalda (3.2 AU, 14°). Later, from dynamical grounds, Jenniskens et al. (2010) concluded that asteroids from the inner asteroid belt (i.e. with orbital semimajor axis  $a < 2.5$  AU) are the likely parent bodies of TC<sub>3</sub>. This reduces the choice to dispersed *B*-class asteroids in the inner main belt and the Polana asteroid group. In Section 2, we revisit this issue studying the possible dynamical source regions for TC<sub>3</sub>.

We recall here that the Polana group is part of a cluster of asteroids known as the Nysa-Polana family (Nesvorný 2010), which is located in the inner main belt, between the  $\nu_6$  secular resonance (at heliocentric distance  $\approx 2.1$  AU) and the 3:1 mean motion resonance with Jupiter (at heliocentric distance of 2.5 AU). This family has a complex – twofold – structure in orbital proper element space (Nesvorný 2010), suggesting that it is the outcome of at least two independent break-up events in the same orbital region. From the few spectral data available at the time, Cellino et al. (2001) argued that the Nysa-Polana family contains asteroids of three spectral classes. The first class is that of *B*-class objects, like asteroid (142) Polana itself – note that Cellino et al. (2001) uses the *F*-class classification from the Tholen (1984) taxonomy; the second class is the *S*-class, with the largest member being identified as the asteroid (878) Mildred; the third class is that of *X*-class objects, such as the asteroid (44) Nysa. In this manuscript, we revisit this result using a much wider dataset of spectro-photometric data provided by the Moving Objects Catalog of the Sloan Digital Survey (SDSS, Ivezić et al. 2002), which is analyzed here using a new classification algorithm (Michel et al. 2005, described in Section 3) developed for the Gaia space mission of the European Space Agency.

A detailed study of the mineralogy of the Nysa-Polana family is of great importance also for better understanding the origin of other NEOs. In particular, Campins et al. (2010) claimed that the asteroid (101955) 1999 RQ<sub>36</sub>, target of the sample return mission OSIRIS-REx (approved in the program New Frontiers of NASA), was delivered to near-Earth space via the  $\nu_6$  secular resonance from the Polana group. Moreover, the binary asteroid (175706) 1996 FG<sub>3</sub>, primary target of the sample return mission Marco Polo-R, under study at the European Space Mission (ESA), might have formed within the Polana group and delivered to the near-Earth space via the overlapping Jupiter 7:2 and Mars 5:9 mean motion resonances rather than the  $\nu_6$  (see Walsh et al. 2012).

As a consequence, in Sections 4 and 5, we perform a spectroscopic analysis using the SDSS data of the asteroids of the Nysa-Polana family as well as dispersed asteroids of the inner Main Belt (called objects of the background) in order to find spectral matches with TC<sub>3</sub> and Almahata Sitta.

Finally, in Section 6, we investigate a possible formation scenario for the TC<sub>3</sub> asteroid as a rubble pile of rocks of different mineralogical types, which is based on the peculiar low inclination of the Nysa-Polana family and dispersed asteroids.

## 2 DYNAMICAL HISTORY AND MAIN-BELT ORIGIN OF TC<sub>3</sub>

The large majority of NEAs are fragments generated by the collisional disruption of larger asteroids of the main belt; said fragments drift in orbital semimajor axis by the so-called Yarkovsky effect until they reach regions of orbital instabilities (mean motion resonances with Jupiter and secular resonances) which, by enhancing their orbital eccentricities, deliver them to the near-Earth space (see Morbidelli et al. 2002, for a review).

According to model by Bottke et al. (2002), there are five main intermediate sources of NEAs:

- 1) the  $\nu_6$  secular resonance, which marks the inner edge of the asteroid belt and occurs when the precession frequency of the longitude of perihelion of an asteroid is equal to that of Saturn;
- 2) the 3:1 mean motion resonance located at  $a \sim 2.5$  AU, where the orbital period of an asteroid is 1/3 of that of Jupiter;
- 3) Mars-Crossing asteroids, defined as objects which are not NEAs (i.e. their perihelion distance  $q$  is larger than 1.3 AU), but whose semimajor axis evolves in a random-walk fashion as a result of close and distant encounters with Mars.
- 4) the outer belt population, whose eccentricities can increase up to planet-crossing values due to a network of high order orbital resonances with Jupiter and three-body resonance of type asteroid-Jupiter-Saturn (Morbidelli & Nesvorný 1999)
- 5) dormant Jupiter family comets.

The orbital elements of TC<sub>3</sub> before impact are not known very precisely. Here are different estimates:  $a = 1.29$  AU,  $e = 0.299$ , and  $i = 2.441^\circ$  (NEODyS website: <http://newton.dm.unipi.it/neodyS>);  $a = 1.308$  AU,  $e = 0.312$ , and  $i = 2.542^\circ$  (Jenniskens et al. 2010). For each of these orbits we computed, using the original orbital evolution files of Bottke et al. (2002), which are the most likely intermediate sources among those enumerated above. We found that TC<sub>3</sub> has a probability of 63-66% to come from the  $\nu_6$  source and 34-37% to come from the Mars crosser population. Apparently, none of the simulations for the 3/1 resonance in Bottke et al. (2002) produce objects within  $\pm 0.05$  AU in  $a$ ,  $\pm 0.05$  in  $e$  and  $\pm 2.5^\circ$  in  $i$  of TC<sub>3</sub>. This contrasts with the claim reported in Jenniskens et al. (2010), that TC<sub>3</sub> has a 20% probability to come from the 3/1 resonance in the Bottke et al. (2002) model. We suspect that there has been an error in the manipulation of the Bottke et al. (2002) model in that work.

Of the Mars crossers that can produce the TC<sub>3</sub> orbit in Bottke et al. (2002) simulations, none has semimajor axis larger than 2.5 AU. From this, and remembering that the  $\nu_6$  resonance lays at the inner edge of the belt, we conclude - in agreement with Jenniskens et al. (2010) - that TC<sub>3</sub> most likely comes from the inner asteroid belt, inside of 2.5 AU.

As noted in Jenniskens et al. (2010), there are two populations of asteroids in the inner belt with spectra broadly consistent with that of TC<sub>3</sub>: the Polana members, with an orbital inclination of 2-3 degrees, and a population of dispersed B-class asteroids, with inclinations ranging up to 15 degrees. These objects are too dispersed to belong to a relatively young collisional family, but their broad cluster in

orbital space suggests that they might belong to an old collisional family, dynamically dispersed probably during the phase when the orbits of the giant planets changed substantially, about 4 Gyr ago.

To determine whether it is more likely that TC<sub>3</sub> comes from the Nysa-Polana family or from the population of dispersed B-class asteroids, we turn, once again, to the original simulations in Bottke et al. (2002). In that work, the initial distribution of asteroids in the  $\nu_6$  was uniform in inclination. In particular, 50% of the initial conditions had initial inclination larger than 8 degrees. However, 93% of the particles which reproduced the orbit of TC<sub>3</sub> at some time during their evolution, have initial inclination  $i < 8^\circ$ . For the Mars crossers, all those reproducing the orbit of TC<sub>3</sub> have initial  $i < 8^\circ$ . This suggests that the most likely source of TC<sub>3</sub> is at low inclination, consistent with the Nysa-Polana family and with the dispersed B-class asteroids with  $i < 8^\circ$ . This is not surprising, given that the inclination of TC<sub>3</sub> is 2.3-2.5 degrees. However, the dynamics rules out a TC<sub>3</sub> origin from the dispersed B-class asteroids at higher inclination (i.e.  $i > 8^\circ$ ).

Finally, Campins et al. (2010) have shown that the Polana group can easily deliver small enough fragments in the  $\nu_6$  resonance. In fact, the extrapolated Yarkovsky-induced semimajor axis distribution of Polana group members predicts that asteroids fainter than  $H \sim 18.5$  can reach the border of the  $\nu_6$  resonance, which is at 2.15 AU for a Polana-like inclination. Assuming a Polana-like geometric visible albedo of 0.05,  $H = 18.5$  translates into a diameter  $D \sim 2$  km, which is much larger than the size of TC<sub>3</sub>.

For all these reasons we conclude that, from the dynamical viewpoint, the Nysa-Polana family and dispersed B-class asteroids with  $i < 8^\circ$  are the most likely sources of TC<sub>3</sub>. Thus, we will focus on the Nysa-Polana family and the Background at low inclination in the next sections.

## 3 SPECTROSCOPIC ANALYSIS METHOD

### 3.1 Asteroid spectral classification algorithm

In order to search for spectral groups in the Nysa-Polana asteroid family or in the inner main belt background at low inclination, we used the unsupervised classification algorithm that will be adopted for the classification of asteroid spectra from the multiband photometers (Jordi et al. 2010) on board the Gaia space mission of the European Space Agency (ESA).

While Gaia is mainly devoted to the observations of  $10^9$  stars, it is expected that this mission will also observe more than 250,000 asteroids multiple times over 5 years (mission lifetime) (Mignard et al. 2007). Spectral classification of asteroids will be performed by an unsupervised classification algorithm based on the works of Michel et al. (2005) and Galluccio et al. (2008). An unsupervised approach has the advantage that no *a priori* information is taken into account to build the spectral groups.

The algorithm is based on a method for partitioning a set  $V$  of  $N$  data points ( $V \in \mathbb{R}^L$ ) where  $L$  in our case is the number of spectral bands into  $K$  non-overlapping clusters (or groups of data points) such that (a) the inter-cluster variance is maximized and (b) the intra-cluster variance is

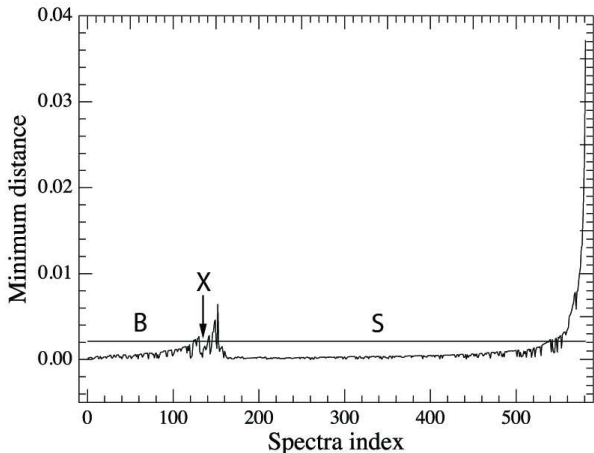


**Figure 1.** Minimum distance between spectra computed by the MST method as a function of the spectra index. The cut off used to obtain the B, X, and S groups was determined such as already classified asteroids belong to their appropriate group.

minimized. Each spectrum is considered as a vertex of tree. A tree is a graph that is connected (i.e. every vertex is connected to at least another vertex) and acyclic (i.e. the graph has no loops). The spanning tree (MST, i.e. the tree passing through each vertex of the set) with the minimal length is calculated using the so-called Prim’s algorithm (see Galluccio et al. 2009, and references therein). The length of each edge of the tree (i.e. the distance between two spectra) is determined using the Kullback-Leibler metric: let  $v_i = \{v_{i1}, \dots, v_{iL}\}$  the feature vector corresponding to a reflectance spectrum ( $L$  being the number of wavelengths); at a given wavelength  $\lambda_j$ , each spectrum is associated with a (positive) normalized quantity:  $\tilde{v}_{ij} = v_{ij} / \sum_{j=1}^L v_{ij}$ , which can be interpreted as the probability distribution that a certain amount of information has been measured around the wavelength  $\lambda$ . To measure the similarity between two probability density functions, we compute the symmetrized Kullback-Leibler divergence:

$$d_{KL}(v_i || v_k) = \sum_{j=1}^L (\tilde{v}_{ij} - \tilde{v}_{kj}) \log \frac{\tilde{v}_{ij}}{\tilde{v}_{kj}}.$$

The identification of the cluster is performed by first computing, at each step of the MST construction, the length of the newly connected edge and then by identifying valleys in the curve obtained by plotting the MST edge length as a function of the iteration of the construction (see Figure 1). The valleys in this curve identify the number and the position of high density region of points, i.e. the clusters (see Galluccio et al. 2009, for a more thorough description of the algorithm).

### 3.2 Spectral data

In order to increase the sample statistics compared to the relatively small number of asteroids observed by Cellino et al. (2001) and identify meaningful spectral groups within the Nysa-Polana family, we used our spectral classification algorithm on the observations contained in the

SDSS MOC4 (Ivezic et al. 2002, <http://www.sdss.org>). The MOC4 contains magnitudes of 104449 Main Belt asteroids. Each asteroid was observed, in general, at multiple epochs over 5 spectral bands in the visible light, namely  $u'$ ,  $g'$ ,  $r'$ ,  $i'$ ,  $z'$  at the following central wavelengths ( $\lambda$ ) of 354, 477, 623, 763, 913 nm, respectively.

To obtain the surface reflectance of the asteroids, we needed to remove the solar contribution ( $u_{\odot}$ ,  $g_{\odot}$ ,  $r_{\odot}$ ,  $i_{\odot}$ ,  $z_{\odot}$ ) to the observed magnitudes. The solar contribution is calculated from transformation equations between the SDSS  $u'g'r'i'z'$  magnitudes and the usual  $UBVR_cI_c$  system. We find:  $u_{\odot} = 6.55$ ,  $g_{\odot} = 5.12$ ,  $r_{\odot} = 4.68$ ,  $i_{\odot} = 4.57$ ,  $z_{\odot} = 4.54$ . (See the SDSS website for more details: <http://www.sdss.org>). In order to compare asteroid spectral reflectances and be able to classify them, we chose to normalize each spectrum relatively to the  $r'$  band ( $\lambda_{r'} = 623$  nm). Finally, we obtained the following asteroid reflectance for the  $\lambda_{u'}$  wavelength:

$$F_{u'} = 10^{-0.4(C_{u'} - C_{r'})}$$

with  $C_{u'} = u' - u_{\odot}$  and  $C_{r'} = r' - r_{\odot}$

the reflectance colors at  $\lambda_{u'}$  and  $\lambda_{r'}$  respectively. The same computations were performed for the  $\lambda_{g'}$ ,  $\lambda_{i'}$ , and  $\lambda_{z'}$  wavelengths.

We searched in the MOC4 database for all asteroids belonging to the Nysa-Polana family and for dispersed objects. Concerning the family members identification, we used the definition of dynamical families of Nesvorný (2010). Among the Nysa-Polana family, 4134 objects have been observed at least once by SDSS (as a comparison, the number of spectra obtained in the visible light or near-infra red, for the Nysa-Polana family, in the SMASS, ECAS and 52-Color catalogs are : 15, 13, and 2, respectively). For those asteroids with more than one observation, we calculated the weighted mean reflectance by averaging the reflectancies derived at each epoch weighing each point with its respective signal-to-noise ratio.

However, likely due to non-photometric conditions some of the observed objects have high uncertainties in the measured magnitudes. In the visible light, the separation of asteroid spectroscopic group is based on the overall slope of their reflectance and in the presence (or absence) and strength of the 1  $\mu$ m absorption feature. In order to avoid the superposition of spectral groups we selected asteroid with the less noisy observations. Namely, we rejected observations with a relative uncertainty  $> 10\%$  on the in-band photometric flux derived from the MOC4 magnitudes. In the end, the taxonomic classification of the Nysa-Polana dynamical family was performed over 579 objects and over 2828 objects for the Background at low inclination.

## 4 SPECTRAL ANALYSIS OF THE NYSA-POLANA FAMILY

### 4.1 Application of the spectral classification method

Figure 1 shows the MST length as a function of the number of iterations (i.e. addition of spectra) in the case of the SDSS-MOC4 spectrophotometric data of the 579 asteroids of the Nysa-Polana family. The figure clearly shows three

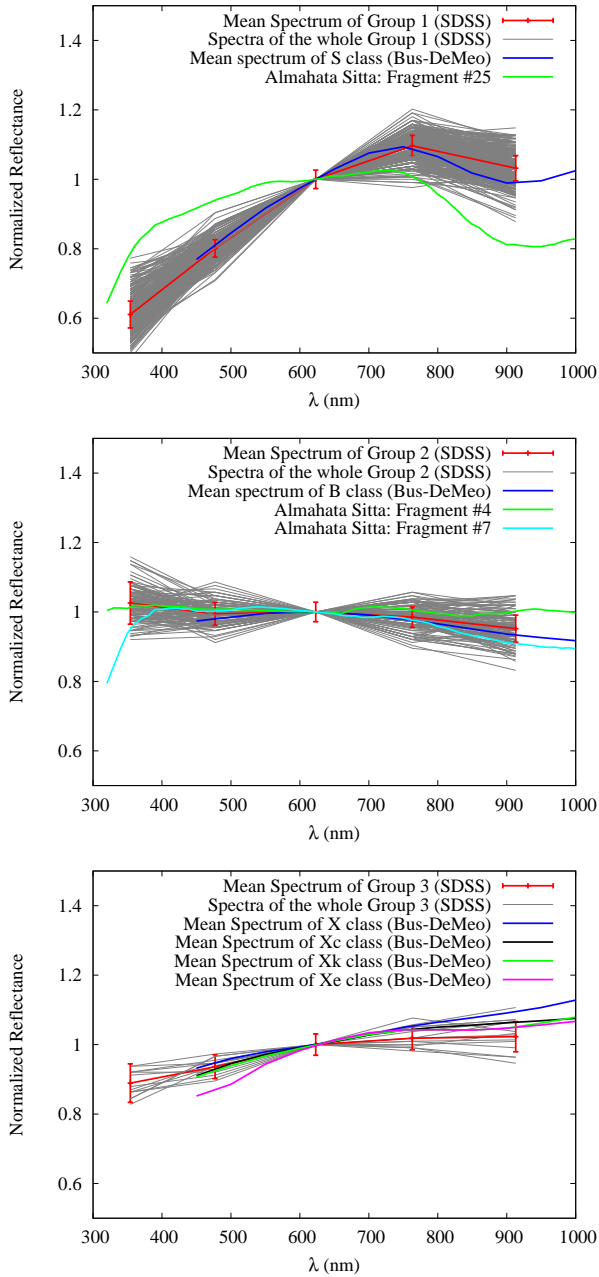


**Figure 2.** Panel (a), (b), and (c) represent the spectra for each group with their mean spectrum. A comparison with several spectra classes coming from the Bus taxonomy is also performed: Group 1 with *S*-class spectrum, Group 2 with *B*-class spectrum and Group 3 with *X*-subclasses. We also find a good agreement with several Almahata Sitta fragments. Spectral differences with fragment #25 (H-chondrite) appearing in panel (a) are likely due to space weathering. Fragments #4 and #7 in panel (b) are ureilites.

main valleys corresponding to three groups composed of 118, 13, and 378 asteroids, respectively. The remaining objects (70) are considered as unclassified asteroids. This is due to their large value of the MST length which means no spectral similarity among the family is found for these 70 objects.

Figure 2 shows asteroid spectra of each group and their average spectrum. Error bars are the 1- $\sigma$  stan-

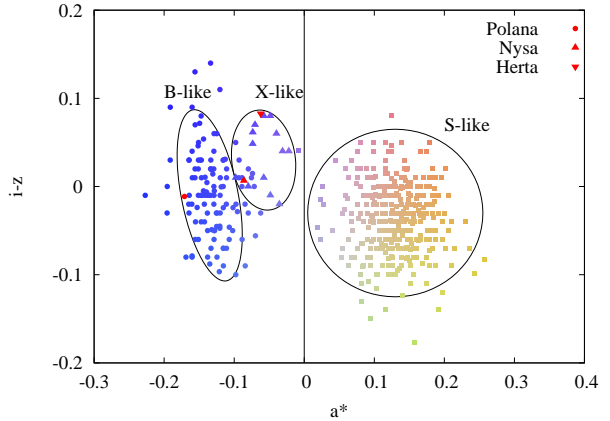


**Figure 3.** Distribution of *S*-class (■), *B*-class (●), and *X*-class (▲) objects of the Nysa-Polana family as a function of  $a^*$  and  $i' - z'$  (calculated from SDSS magnitudes). Ellipses represent the location of *S*, *B*, and *X* regions. The color palette is the same of Parker et al. (2008). Although Polana (*B*), Nysa (*X*), and Herta (*X*) have not been observed by SDSS, we have calculated their  $a^*$  and  $i' - z'$  values from the ECAS catalog and located them in this plot.

dard deviation. We also compared the spectra of each spectral group of asteroids with the mean spectrum of different taxonomic classes from the Bus classification (<http://smass.mit.edu/busdemeoclass.html>). In each panel, we only plot the Bus mean spectra which present the closer similarity with the mean spectra of each group:

(i) For the first group (top panel of Figure 2, 378 objects), we find that all spectra resemble the *S*-class mean spectra of Bus.

(ii) In the middle panel of Figure 2, the 118 spectra of the second group fits with *B*-class asteroids (such as 142 Polana, for instance).

(iii) The bottom panel shows the third more populous group containing 13 asteroids. Comparing the spectra of this group and the mean spectrum of the *X*-class, *X<sub>c</sub>*-class, *X<sub>k</sub>*-class, and *X<sub>e</sub>*-class, we find that the third group of 13 objects corresponds to asteroids of the *X*-complex and its subclasses.

We note that groups (1) and (2) are consistent with the two main spectral classes found by Cellino et al. (2001). Moreover, the same authors had already identified the presence of asteroids with *X*-class spectral reflectances. They also noted that two of the largest asteroids, (44) Nysa and (135) Herta have spectra consistent with an *X*-class. As a consequence, we confirm their results using the SDSS MOC4 large sample of spectra.

In Figure 3 we plot the asteroids of the three spectroscopic groups of the Nysa-Polana family as a function of  $a^*$  and  $i' - z'$  (with  $a^* = 0.89(g' - r') + 0.45(r' - i') - 0.57$ ). We show that the *S*-class group is well defined with  $a^* \in [0; 0.25]$  and  $i' - z' \in [-0.15; 0.08]$ . The *B*-class region stretches from  $\sim -0.2$  to  $\sim -0.06$  for  $a^*$  and from  $-0.1$  to  $0.14$  for  $i' - z'$  and we find for the *X*-class region,  $a^* \in [-0.1; -0.02]$  and  $i' - z' \in [-0.02; 0.08]$ . The color palette used in Fig. 3 is that of Parker et al. (2008). Blue dots correspond to asteroids with neutral or slightly blue spectra (*B*-class), asteroids

with neutral to slightly red spectra (X-class) are displayed in the plot with purple colors, while S-class asteroids are red to yellow.

#### 4.2 Comparison with Almahata Sitta meteorites

It is very interesting to note that the three asteroid spectroscopic groups that we found in the Nysa-Polana family are likely to be the analogs of the different meteorite mineralogies found in Almahata Sitta. To strengthen this argument, we also compare – in Figure 2 – the mean spectrum of each asteroid spectroscopic class of the Nysa-Polana family (S, B, X; red curves) with published spectra (from Hiroi et al. 2010) of some fragments of Almahata Sitta. We note that at the time of writing, spectra of E-chondrites from Almahata Sitta are not yet publicly available. So, comparisons between the classes of asteroids in the Nysa-Polana family and fragments of Almahata Sitta were performed for the S and B classes only. However, comparison of spectra of other E-chondrites (from the RELAB database from Gaffey 1976) with the average spectrum of the the Nysa-Polana X-class shows a good agreement.

Concerning the B class, we find that the mean spectrum of the Nysa-Polana B-class asteroids matches the spectra of the fragments #4 and #7 (ureilites) of Almahata Sitta. It is important to note that this spectral match was obtained only considering the visible wavelengths between about 350 and 900 nm. We remind that, from spectroscopic and albedo similarities, Jenniskens et al. (2009, 2010) have proposed a link between the B-class (or the F-class) and ureilite meteorites. An important caveat is that the link between B-class asteroids and the Almahata Sitta ureilites proposed by Jenniskens et al. (2009, 2010) is based on the noisy spectrum of TC<sub>3</sub>. Moreover, B-class asteroids are more commonly associated with carbonaceous chondrites by several studies (see Clark et al. 2010, for a review about B-class objects, their meteorite analogues and their composition). However, a recent spectroscopic survey of B-class asteroids by De Leon et al. (2012) shows that the ensemble of the reflectance spectra of the 45 B-class asteroids analyzed in their work have a continuous shape variation in the range between 500 and 2500 nm, from a monotonic negative (blue) slope to a positive (red) slope. De Leon et al. (2012) apply a clustering technique to reduce the ensemble of the spectra to 6 optimized averaged spectra or “groups”. Interestingly the RELAB spectrum of the fragment #4 of Almahata Sitta shows a good match with the group #3 of De Leon et al. (2012) in the region between 500 and 2500 nm (De Leon, J. private communication September, 2011).

Concerning the S class, we show, in Fig. 2, that fragment #25 (an ordinary chondrite) is rather close to the S-class mean spectrum, as expected, but not in very good agreement (see e.g. the review of Chapman 2004, for spectroscopical links between ordinary chondrites and S-class asteroids). One possible explanation for this spectral mismatch is the space weathering of S-class asteroids. We discuss this possibility in the following subsection.

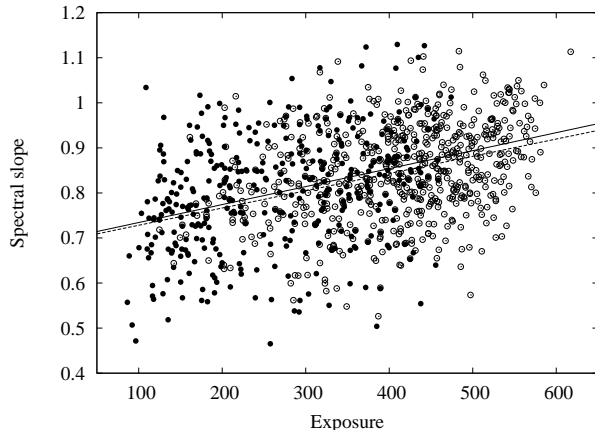


**Figure 4.** Spectral slope as a function of the exposure to space weathering of S-class objects of the Nysa-Polana family (black dots and black line) and S-class objects of the background at low inclination (circles and dashed line). As a comparison, the spectral slope of H-chondrites which are thought to come from S-class asteroids is of about 0.1 – 0.2.

#### 4.3 Space weathering of S-class members of the Nysa-Polana family

Space weathering is a physical process caused by cosmic rays, collisions, ion bombardment, that alters physical and spectral properties of the surface of atmosphere-less planetary bodies. More particularly, due to space weathering, S-class asteroids become darker (their albedo is reduced), redder (the reflectance increases with increasing wavelength), and the depth of absorption bands are reduced. As a consequence, the spectral slope changes due to this process (Clark et al. 2002; Chapman 2004).

In Marchi et al. (2006), a strong relation was found between the spectral slope of S-class asteroids and their “exposure” to space weathering. The exposure of an asteroid to space weathering corresponds to time integral the flux of solar ions that the body receives along its orbit. The exposure to space weathering depends on the age of the asteroid and its average distance from the Sun. Therefore, in order to know if space weathering affected S-class asteroids of the Nysa-Polana family, we calculate the exposure to space weathering of these bodies as shown in Marchi et al. (2006) and Paolicchi et al. (2007).

We compute the slope  $\alpha$  of a SDSS spectrophotometric data by fitting a linear equation normalized to 1 at  $\lambda_r$  (623 nm) to the datapoints. To calculate the exposure, we need to estimate the average collisional age of Main Belt asteroids ( $T_{MBA}$ ), which can be constrained by the age of the Belt ( $t_{LHB} \sim 4$  Gyr) and by collisional times ( $\tau_{coll}$ ):

$$T_{MBA} \simeq \tau_{coll} \left[ 1 - \left( 1 + \frac{t_{LHB}}{\tau_{coll}} \right) e^{-\frac{t_{LHB}}{\tau_{coll}}} \right] + t_{LHB} e^{-\frac{t_{LHB}}{\tau_{coll}}}$$

According to Bottke et al. (2005), the collisional lifetime can be estimated as a function of asteroid diameter (using SDSS H absolute magnitudes and assuming an albedo of  $\rho_V = 0.2$  for all S-class objects). In the end, we have:

$$\text{exposure} \propto \frac{T_{MBA}}{a^2 \sqrt{1 - e^2}}$$

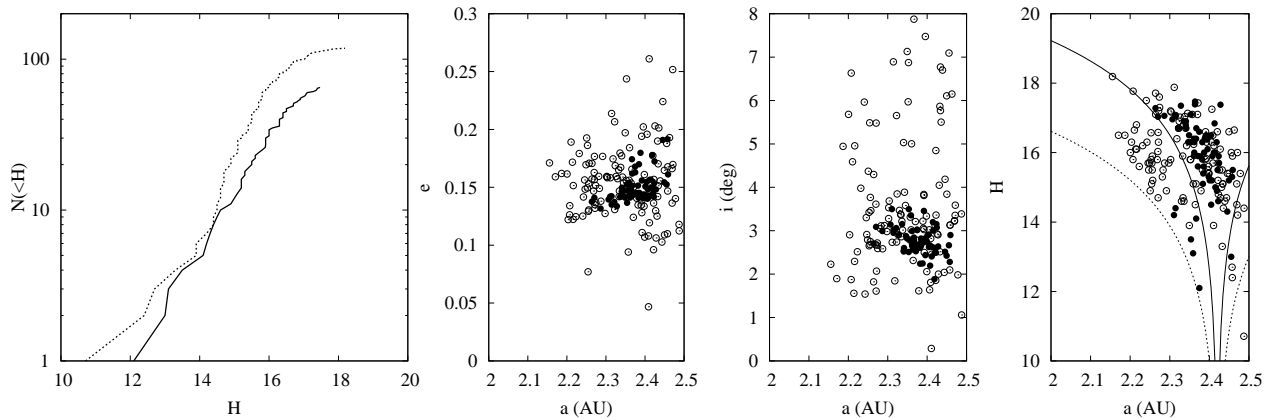


**Figure 5.** Plot 1: Cumulative number of asteroid  $N(<H)$  as a function of the  $H$  absolute magnitude for B-class asteroids of the Nysa-Polana family (black curve) and the Background at low inclination ( $i < 8^\circ$ ; dashed curve). Plot 2-4: Distribution in eccentricity (plot 2), inclination (plot 3) and  $H$  absolute magnitude (plot 4) as a function of semimajor axis. Black points correspond to Polana B-class asteroids and black circles to B-class dispersed objects from the Background at low inclination. Plot 4 shows the  $H$ -dependent semimajor axis distribution induced by the Yarkovsky effect that best fits the boundaries of the observed distribution for the Polana group (black curves) and for the Background at low inclination (dashed curve).

with  $a$  and  $e$  the asteroid proper semimajor axis and eccentricity, respectively.

In Figure 4, we plot both the spectral slope of Nysa-Polana S-class objects as a function of the exposure to space weathering and the best linear fit to this distribution. The two-tailed probability for the linear correlation is lower than 0.001% which means the linear correlation is significant<sup>1</sup>. This shows that the spectral slope increases with the exposure.

Semimajor axes and eccentricities do not vary much within the Nysa-Polana family. As a consequence, the exposure variation mainly comes from asteroid diameter, through the computation of  $T_{MBA}$ . Hence, plotting the spectral slope as a function of the exposure, or  $T_{MBA}$ , or asteroid diameters ( $d$ ) provide quite similar figures (not shown here) – where the exposure increases with time or diameter – but with the following abscissa ranges:  $0.5 < T_{MBA} < 2.5$  Gyr or  $1 < d < 6$  km.

The spectral slope increase with exposure or asteroid age is then the proof that space weathering occurs for S-class asteroids of the Nysa-Polana family. We also note that the spectral slope of the fragment #25 of Almahata Sitta has the value of 0.03.

As a consequence, the spectral mismatch between asteroids of the S-component of the Nysa-Polana family and the ordinary chondrites of Almahata Sitta – as observed in Figure 2 – can be explained by space weathering.

## 5 ANALYSIS OF ASTEROIDS OF THE BACKGROUND AT LOW INCLINATION

As mentioned in Sections 1 and 2, the other possible origin source for TC<sub>3</sub>, from a dynamical point of view, is the population of dispersed asteroids at low inclination. In the present section, we perform the same spectroscopic study

as for the Nysa-Polana family (Section 4) but using objects of the Background located in the Inner Main Belt ( $2.1 < a < 2.5$  AU) with a proper inclination lower than  $8^\circ$ . Selecting the best observations of the SDSS MOC4 catalog (i.e. observations with a relative uncertainty  $> 10\%$  on the in-band photometric flux, corresponding to 2828 objects), we find 4 large groups of asteroids corresponding to the following spectral classes: B, C, X, S, as well as small clusters of Q, V, and A-class asteroids. In addition, for the B, X, and S groups of the Background, we obtain mean spectra very similar to those of the Nysa-Polana family (not shown here). We also note that space weathering is also found for S-class asteroids of the Background (see Fig. 4). As a consequence, the three ingredients required to form TC<sub>3</sub> (S-class asteroid/H-chondrite; B-class asteroid/ureilite; X-class asteroid/enstatite chondrite) are both found in the Nysa-Polana family and in the Background at low inclination.

In our attempt to definitively conclude on the origin region of TC<sub>3</sub>, we have compared the distribution of B-class asteroids for the two source regions. In order to get a homogeneous selection of B-class asteroids both from the Nysa-Polana family and the Background at low inclination, we have selected objects such as their spectra are similar to the B-class mean spectrum of the Nysa-Polana family, within the  $1-\sigma$  error bar. Although this selection reduces the size of the original B-class groups, we limit the overlap of classes (B and X classes can overlap; see Fig. 2).

From this selection, we plot in Fig. 5, the cumulative number of asteroids as a function of  $H$  absolute magnitude as well as the distribution in eccentricity, inclination and  $H$  magnitude as a function of semimajor axis. We find more B-class asteroids from the Background at low inclination (dashed curve in the first plot of Fig. 5) than from the Polana group (black curve). As a consequence, the Background at low inclination seems to dominate the Polana group, even if, around magnitude 17, the slope of the Polana group curve looks a little steeper than the curve for the Background. In the other plots in orbital elements, we can see that the two regions overlap in some points and that B-class objects

<sup>1</sup> A linear fit is considered significant whenever the two-tailed probability is lower than 5%.



of the Background are much more dispersed compared to Polana asteroids.

As in Campins et al. (2010), we also represent the absolute magnitude ( $H$ ) as a function of semimajor axis, both for the Polana group and the Background (the plot of Campins et al. 2010, was done for the whole Nysa-Polana family). The plot appears to be V-shaped which is a feature known to be associated both with the size-dependent ejection velocity field and with the drift in the proper semimajor axis induced by the Yarkovsky effect (e.g. Vokrouhlický et al. 2006). In the plot, the black curve shows the  $H$ -dependent semimajor axis distribution induced by the Yarkovsky effect that best fits the boundaries of the observed distribution for the Polana B-class asteroids. Objects below this curve are expected to be interlopers and may belong to the Background. The extrapolated Yarkovsky-induced distribution predicts that the Polana group should reach the outer edge of the  $\nu_6$  resonance for objects with  $H \sim 18$ , which for a Polana-like albedo of  $p_v = 5\%$  translates into a diameter  $D \sim 2$  km. This means that objects smaller than 2 km, such as TC<sub>3</sub>, can easily escape the Polana group and the Inner Main Belt.

Concerning the Background at low inclination, different size limits can be computed due to a large variation of proper orbital inclinations. For an inclination of  $\sim 0^\circ$ , the  $\nu_6$  resonance boundary is found at  $a \sim 2.1$  AU, which gives us an  $H$  magnitude of  $\sim 16$  and an asteroid diameter limit of  $d \sim 4$  km. For the highest inclination ( $i \sim 8^\circ$ ), we obtain  $H \sim 14.5$  at  $a \sim 2.2$  AU, which is equivalent to a B-class asteroid ( $p_v = 5\%$ ) of 8 km. As a result, the Background at low inclination could have also delivered TC<sub>3</sub> through the  $\nu_6$  resonance.

Because the Background at low inclination is not a dynamical family, its V-shaped structure in  $H(a)$  was not especially expected. We then think that the Background at low inclination could correspond to an old break-up of the Nysa-Polana family. As a consequence, we can conclude that TC<sub>3</sub> comes from the Inner Main Belt, more particularly from the Background at low inclination or the Nysa-Polana family, and that these two sources could be genetically linked.

## 6 POSSIBLE FORMATION SCENARIO OF 2008 TC<sub>3</sub>

Meteorite strewn fields with fragments of different mineralogical types are very rare. Almahata Sitta and Kaidun (Ivanov et al. 1984) are probably the only known specimen. In the scenario that mixing occurs by a collisional process, the paucity of mineralogically-mixed meteorites suggests that the process that formed Almahata Sitta i.e. mixing the material between projectile and target is very rare; in most cases the projectile is pulverized and leaves negligible traces in the target (Melosh 1989).

It is unclear which conditions allow for mixing between projectile and target. Impact velocity is probably a key parameter. The average impact velocity between asteroids in the main belt is 4.4-5.3 km/s (Bottke et al. 1994). If projectile/target mixing were possible at these impact speeds, meteorites like Almahata Sitta would probably be frequent, which is not the case. Thus, we think that unusually low impact velocities are needed for mixing. This could prevent

the target from pulverizing and could lead to macroscopic projectile fragments being implanted in the regolith of the impacted body or gravitationally bound to fragments of the target, if the latter is catastrophically disrupted by the impact. The fact that we give evidence that TC<sub>3</sub> comes from the Nysa-Polana family (see Section 4) or the Background at low inclination (see Section 5), which are characterized by a mixing of taxonomic classes, also suggests that a specificity of the members of these families/regions may be unusually low collision velocities with projectiles that are also on low-inclination orbits.

For all these reasons we did a systematic search for projectiles that could hit Nysa-Polana family members or dispersed asteroids of the Background at very low speeds. We did this search using the algorithm for the calculation of the intrinsic collision probability  $P_i$  between pairs of asteroids, described in Wetherill (1967). This algorithm, given the semimajor axis  $a$ , eccentricity  $e$  and inclination  $i$  of the two orbits (we use proper values for each pair of selected asteroids) assumes that the angles  $M$ ,  $\omega$ ,  $\Omega$  (mean anomaly, argument of perihelion and longitude of the ascending node) of the two objects have a uniform probability distribution over the range  $0 - 2\pi$ ; then it computes which fraction of these angles corresponds to the two objects being closer to each other than 1 km; finally, this fraction is translated into an intrinsic collision probability per year ( $P_i$ ), using the orbital periods of the two objects and assuming that they are not in resonance with each other. For our goals, we modified this algorithm in order to take into account only orbital intersections corresponding to relative speeds smaller than 0.5 km/s. Admittedly, this velocity threshold is arbitrary. Given the exceptional character of Almahata Sitta, we need a threshold much smaller than the typical impact velocity among random asteroids, that is to say a sub-sonic impact velocity, in order to preserve the target.

Because most of Almahata Sitta fragments recovered are mainly made of ureilites, which we consider as analogs of B-class asteroids (as previously mentioned in Section 1 and according to Jenniskens et al. 2010), we assume that the favorite scenario for the formation of TC<sub>3</sub> involves a low velocity collision of asteroids of X and S classes (projectiles) with a B-class member (target) of the Nysa-Polana family.

As for projectiles we considered all asteroids known in the ASTORB file (Asteroid Orbital Elements Database: <ftp://ftp.lowell.edu/pub/elgb/astorb.html>) of the whole Main Belt and we computed the probability of collision of each asteroid with a B-class object near the center of the B-class group of the Nysa-Polana family. Figure 6 shows the region of orbital element space where impacts can occur (impact probability  $>0$ ). This figure shows that asteroids included in the region of low-velocity impacts have different SDSS colors and thus different taxonomies. As a consequence, collisions involving B-class, S-class, and X-class asteroids are likely to be possible.

In the end, depending on the location of the target within the Polana group, we find that projectiles come from one of the following families: (i) Nysa-Polana, (ii) Flora or (iii) Massalia, located in the inner Main Belt, or (iv) Hestia which is in the central Main Belt, very close to the 3:1 mean motion resonance with Jupiter. More particularly, for targets with a semimajor axis ( $a$ ) smaller or equal than 2.3 AU, the Flora family and objects of the background, very close to the



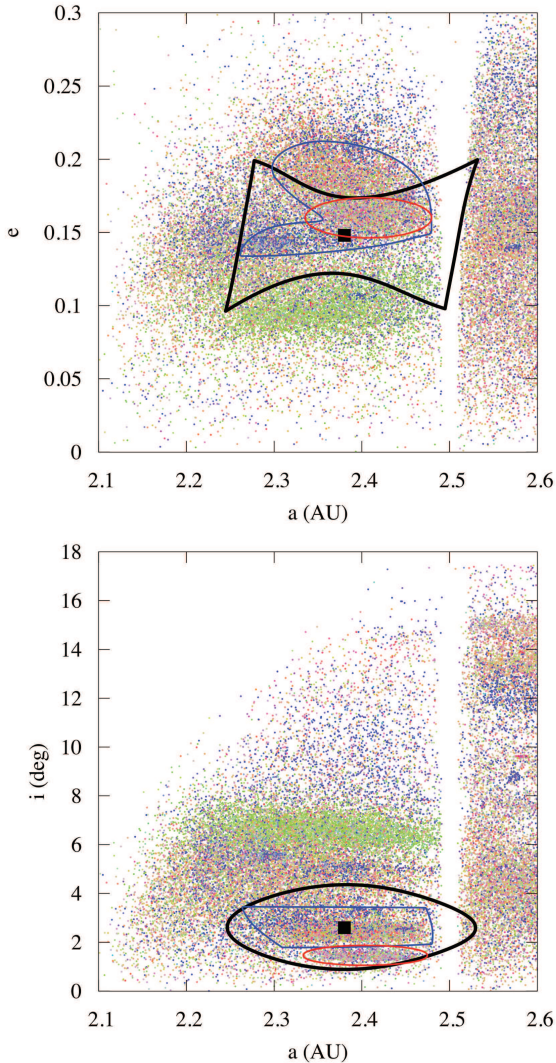


**Figure 6.** Distribution of proper orbital element for asteroids of the inner Main Belt: semimajor axes and eccentricities (top panel) or inclinations (bottom panel). For an asteroid target (black square), the region of orbital element space where impactors can come from is plotted in black. The location of the Nysa-Polana and Massalia families are respectively represented in blue and red. The color palette corresponds to the Parker’s color distribution as mentioned in Parker et al. (2008) and depends on the value of  $a^*$  and  $i' - z'$ , with  $a^* = 0.89(g' - r') + 0.45(r' - i') - 0.57$ ,  $g'$ ,  $r'$ ,  $i'$ ,  $z'$  corresponding to SDSS magnitudes at the following central wavelengths: 477 nm, 623 nm, 763 nm and 913 nm, respectively. Bluer dots ( $a^* \in [-0.25; 0]$  and  $i' - z' \in [-0.2; 0.2]$ ) are related to dark objects while yellow to red colors ( $a^* \in [0; 0.25]$  and  $i' - z' \in [-0.2; 0.2]$ ) gather brighter objects (see Figure 3 for more details). Data come from the SDSS Moving Objects Catalog 4.

Flora and Nysa-Polana family are the main source of projectiles; for targets with  $2.3 < a < 2.4$  AU and eccentricities larger than  $\sim 0.15$ , projectiles in general are likely to come from the Nysa-Polana family; for targets with  $2.3 < a < 2.4$  AU and eccentricities smaller than  $\sim 0.15$ , projectiles are likely to come from the Massalia family; for targets with  $a \geq 2.4$  AU projectiles come from the Hestia family. Similar

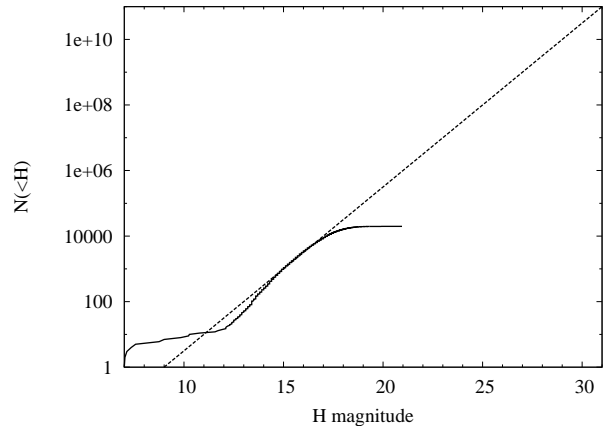


**Figure 7.** Size frequency distribution (SFD) of the asteroid population in the impact region. The SFD is plotted in terms of the cumulative number of asteroid as function of their absolute magnitude ( $H$ ).

results are found when studying collisions involving B-class asteroids of the Background at low inclination.

Once identified the region of potential impactors, we proceeded to estimate the likelihood and the frequency of impacts, which depend on the sizes, number density of asteroids, and average impact probability in the region. The average impact probability in the region was derived by averaging the intrinsic impact probabilities (one of the output of our algorithm) of the asteroids in the region; we found  $P_i = 3 \cdot 10^{-19}$  impacts/km<sup>2</sup>/year.

First of all, we estimated the number of impacts and the size of the impactors hitting TC<sub>3</sub> during its collisional lifetime assuming a diameter of 4 m (given by its  $H$  value of 30.9 (Jenniskens et al. 2009) and assuming a geometric visible albedo of 0.05). The impact probability per projectile for TC<sub>3</sub> is given by  $P_p = R^2 \tau_{coll} P_i$  with  $R$  the radius of TC<sub>3</sub> and  $\tau_{coll}$  its collisional lifetime estimated from Marchi et al. (2006) ( $\tau_{coll} = 16.2$  Myr). As a consequence, we find that TC<sub>3</sub> has an impact probability per projectile of the order of  $2 \cdot 10^{-17}$  during its collisional lifetime.

To obtain the number of impacts on TC<sub>3</sub> during its collisional lifetime, we estimated the number of projectiles by calculating the size frequency distribution (SFD) of the population of the asteroids in the impact region and extrapolating the corresponding function to asteroid sizes below the detection limit of current discovery surveys. Figure 7 shows the SFD in terms of the cumulative number of asteroid as function of their absolute magnitude ( $H$ ). We used  $H$  values from the ASTORB file. In order to extrapolate the SFD asteroid sizes below the current detection limits, we calculated the equation of the straight line that best fits the base-10 logarithm of the known SFD and that is compatible with the size frequency distribution of the whole Main Belt (see Bottke et al. 2002) (see Figure 7). The line has equation  $y = \alpha H + \beta$  where  $y$  is the  $\log_{10}(N(> H))$  10-base logarithm of the cumulative number of asteroids with  $H$  smaller or equal than a threshold value. The best-fit value for  $\alpha$  and  $\beta$  are 0.5 and -4.5 respectively, implying about  $10^4$  asteroids with  $H < 17$ ,  $10^6$  objects with  $H < 21$ ,  $10^9$  with  $H < 27$  and  $10^{11}$  with  $H < 31$ , if the linear extrapolation is

assumed to be valid. We can deduce that for  $H < 31$ , we obtain only  $\sim 10^{-6}$  impacts with TC<sub>3</sub>. In the end, 1 impact at  $v \leq 0.5$  km/s during TC<sub>3</sub> collisional lifetime would require  $1/P_p$  objects (i.e.  $5 \cdot 10^{16}$  objects). Using the SFD equation, this means we need a collision with an object of magnitude  $H \sim 42$ . This correspond to the size of a pebble of 2.4 cm of diameter. Clearly the contamination brought by low speed impacts is very small (the volume ratio between TC<sub>3</sub> and the pebble is  $1.1 \cdot 10^{-7}$ ) and certainly not at the level of 20-30% as implied by the number of chondrites found amongst the ureilites of the Almahata Sitta meteorites.

Much more likely, TC<sub>3</sub> was a fragment of a larger asteroid that was liberated by an impact near the  $\nu_6$  resonance few millions years ago. In fact, we note that (1) the dynamical time to deliver asteroids from the  $\nu_6$  resonance to orbits similar to that of TC<sub>3</sub> is of the order of 19 Myr (see Campins et al. 2010, for 1999 RQ<sub>36</sub> coming from the Polana region); (2) the cosmic ray exposure age of Almahata Sitta meteorites is of  $19.5 \pm 2.5$  Myr (Welten et al. 2010); as a consequence, TC<sub>3</sub> spent most of its life as a single asteroid traveling from the  $\nu_6$  resonance to the orbit that brought it to impact the Earth.

It makes sense to investigate what was the contamination brought by low velocity impacts on the parent body of TC<sub>3</sub>. The average impact probability implies that we have  $\sim 1.4 \cdot 10^{-9}$  impacts/km<sup>2</sup> over the age of the Solar System, which correspond to 1 impact of an asteroid of  $H \sim 27$  taking into account the SFD of the objects in the region. The diameter of an asteroid with  $H=27$  is between 10 and 25 m depending on the albedo. Again the level of contamination is very little, of the order of  $1 \cdot 10^{-5}$ .

When we take into account the necessity of mixing meteorites of at least three different mineralogies, we conclude that the formation of TC<sub>3</sub> by means of low-velocity collisions is not a realistic scenario.

## 7 CONCLUSION

From our study, it seems that the Nysa-Polana family and the Background at low inclination are good candidates for the origin of 2008 TC<sub>3</sub> and Almahata Sitta. First of all, as mentioned in Section 2, the Nysa-Polana family is located close to the  $\nu_6$  secular resonance which is the favorite route leading to primitive NEOs and more particularly to asteroid 2008 TC<sub>3</sub>. Moreover, the proper inclination of the Nysa-Polana family is very similar to that of TC<sub>3</sub>, which should have been maintained during the transfer of TC<sub>3</sub> to the NEOs region through the  $\nu_6$  secular resonance. We also know, from our algorithm of spectral classification (Section 3), that the Nysa-Polana family gathers the 3 spectral classes (S, B, and X), which are proposed analogs to Almahata Sitta fragments (Section 4) under the hypothesis that ureilites are linked to B-class asteroids. More specifically, (1) the mean spectrum of B-class asteroids of the Nysa-Polana family is spectrally matched – at least in the visible – with available spectra of ureilitic fragments of Almahata Sitta, (2) considering space-weathering effects, the mean spectrum of S-class asteroids of the Nysa-Polana family is compatible with the spectrum of the H-chondrite fragment #25, (3) a good agreement is found between X-class asteroids and enstatite chondrites from other meteorite falls (we remind

that enstatite chondrites are part of Almahata Sitta). Of course, a comparison with enstatite chondrites from Almahata Sitta fragments would be very useful to get a definitive match between the Nysa-Polana family and Almahata Sitta. In Section 5, the same kind of work was performed for objects of the inner Main Belt coming from the Background at low inclination ( $i < 8^\circ$ ). We concluded that these dispersed asteroids could also be at the origin of TC<sub>3</sub>.

In Section 6, we tried to explain the formation of TC<sub>3</sub> by low velocity impacts (below 0.5 km/s) between different mineralogies in the neighborhood of and within the Nysa-Polana family. Selecting TC<sub>3</sub> as the target asteroid ( $d=4$  m), we find a probability per projectile about  $10^{-17}$  impacts during its collisional lifetime (i.e. in 16.2 Myr). As a consequence, impacts at low velocity are extremely rare and there is little chance that TC<sub>3</sub> was formed by low-velocity impacts in the current asteroid belt. This implies that the heterogeneous composition of the parent body of TC<sub>3</sub> has to be inherited from a time when the asteroid belt was in a different dynamical state, most likely in the very early Solar System. One could think that an asteroid of ureilite composition was contaminated by impactors of different nature when the asteroid belt was still massive and dynamically cold, so that mutual collisions were frequent and at low velocity. However, this view is probably simplistic. In fact, a body of ureilite composition needs to be formed in the interior of a large carbonaceous asteroid which underwent significant thermal alteration (Singletary & Grove 2003). This asteroid needs to have undergone a collisional disruption to expose the ureilite material in space. The same is true for the bodies of Hn composition, with n larger than 3 (Gopel et al. 1993). But collisional disruptions require large relative velocities, in contrast with the view of a dynamically cold belt. Thus, the asteroid belt could not be overall dynamically cold when the parent body of TC<sub>3</sub> formed.

These considerations suggest that, conversely to what is usually thought, accretion and collisional erosion had to co-exist for some time in the asteroid belt. For this to be possible, presumably there had to be still a significant amount of gas in the system so that, although large asteroids could be on dynamically excited orbits, the orbit of their small fragments were rapidly re-circularized by gas-drag. Consequently, the mutual relative velocities of these fragments were small and a new phase of accretion was possible for them.

We remark that the heterogeneity of TC<sub>3</sub> is not at the microscopic level; each of the meteorites delivered to the ground are of a distinct class. Thus, TC<sub>3</sub> seems to be an agglomeration of meteorite-sized (i.e. few dm) pebbles of different nature. Pebbles of this size are strongly coupled with the gas and are extremely sensitive to pressure gradients. They play the key role in the new models of planetesimal formations, based on the concentration of dm-size pebbles in the eddies of a turbulent disk and on the process of streaming instability (Johansen et al. 2007, 2009). These models of planetesimal formation in a turbulent disk seem a priori to be particularly favorable to explain the coexistence of collisional erosion and accretion. Large planetesimals are formed by the concentration of a large number of pebbles, forming self-gravitating clumps. Once formed, the orbits of these large planetesimals are rapidly excited by the stochastic gravitational perturbations exerted by the tur-

bulent disk (Ida et al. 2008; Morbidelli et al. 2009). If the threshold for collisional break-up is achieved, the pebble-size fragments of these large bodies are re-injected into the game: by being concentrated into new eddies they can give origin to new large planetesimals and so forth. Admittedly, quantitative work is needed to support this scenario; also, other more classical planetesimal formation mechanism in presence of gas drag (Wetherill & Stewart 1993; Kenyon & Bromley 2004; Weidenschilling 2011) might explain the coexistence of erosion and accretion as well.

In this respect, it will be important to understand from the observational point of view if macroscopic heterogeneity as that of TC<sub>3</sub> is the exception or the rule among asteroids. TC<sub>3</sub> is the first object of this kind that has ever been observed, but it is also the first fall of an asteroid on Earth documented live and for which an extensive and exhaustive search for meteorites has been done. So, it might not be as rare as one could be tempted to believe. Indeed, a second similar case has just been reported (Spurný et al. 2012). Now that the possibility for macroscopic heterogeneity is recognized, careful investigations (also conducted by remote sensing techniques) may reveal additional interesting cases. Understanding which fraction of the asteroids are of primary or secondary accretion will be a fundamental step to constrain the asteroid formation and evolution models.

## 8 ACKNOWLEDGEMENTS

We thank O. Michel and P. Bendjoya for providing us their method of classification as well as A. Cellino, P. Tanga, M. Müller, H. Campins, B. Carry, and P. Vernazza for helpful discussions. Programming tools made available to us by the Gaia Data Processing Analysis Consortium (DPAC) have been used within this work. J. Gayon-Markt is also grateful to the Centre National d'Etudes Spatiales (CNES) for financial support.

## REFERENCES

Binzel, R. P., & Xu, S. 1993, *Science*, 260, 186  
 Bischoff, A., Horstmann, M., Pack, A., Laubenstein, M., & Haberer, S. 2010, *Meteoritics and Planetary Science*, 45, 1638  
 Bottke, W. F., Nolan, M. C., Greenberg, R., & Kolvoord, R. A. 1994, *Icarus*, 107, 255  
 Bottke, W. F., Morbidelli, A., Jedicke, R., Petit, J.-M., Levison, H. F., Michel, P., & Metcalfe, T. S. 2002, *Icarus*, 156, 399  
 Bottke, W. F., Durda, D. D., Nesvorný, D., Jedicke, R., Morbidelli, A., Vokrouhlický, D., & Levison, H. 2005, *Icarus*, 175, 111  
 Bus, S. J. & Binzel, R. P. 2002, *Icarus*, 158, 146  
 Campins, H., Morbidelli, A., Tsiganis, K., de León, J., Licandro, J., & Laretta, D. 2010, *ApJL*, 721, L53  
 Cellino, A., Zappalà, V., Doressoundiram, A., di Martino, M., Bendjoya, P., Dotto, E., & Migliorini, F. 2001, *Icarus*, 152, 225  
 Chapman, C. R. 2004, *Annual Review of Earth and Planetary Sciences*, 32, 539

Clark, B. E., Hapke, B., Pieters, C. & Britt, D. 2002, in *Asteroids III* (eds Bottke, W. F., Cellino, A., Paolicchi, P. & Binzel, R. P.) 585599 (Univ. Arizona Press, 2002).  
 Clark, B. E., Ziffer, J., Nesvorný, D., Campins, H., Rivkin, A. S., Hiroi, T., Barucci, M. A., Fulchignoni, M., Binzel, R. P., Fornasier, S., DeMeo, F., Ockert-Bell, M. E., Licandro, J., Mothé-Diniz, T. 2010, *Journal of Geophysical Research (Planets)*, 115, 6005.  
 Cloutis, E. A., Hudon, P., Romanek, C. S., Bishop, J. L., Reddy, V., Gaffey, M. J., & Hardersen, P. S. 2010, *Meteoritics and Planetary Science*, 45, 1668  
 De Leon, J., Pinilla-Alonso, N., Licandro, J., Campins, H., & Marzo, G. A. 2012, *Icarus*, 218, 196  
 Gaffey, M. J. 1976, *Journal of Geophysical Research*, 81, 905  
 Gaffey, M. J., Burbine, T. H., Piatek, J. L., Reed, K. L., Chaky, D. A., Bell, J. F., & Brown, R. H. 1993, *Icarus*, 106, 573  
 Galluccio, L., Michel, O., Bendjoya, P., & Slezak, E. 2008, in *AIP Conf. Ser. Vol. 1082, Classification and Discovery in Large Astronomical Surveys*. Am. Inst. Phys., New York, p. 165  
 Galluccio, L., Michel, O., Comon, P., Slezak, E., & Hero, A.O. 2009, Technical Report I3S/RR-2009-08FR, CNRS and Nice-Sophia Antipolis University, France.  
 Gopel, C., Manhes, G., & Allegre, C. J. 1993, *Meteoritics*, 28, 354  
 Hiroi, T., Jenniskens, P., Bishop, J. L., Shatir, T. S. M., Kudoda, A. M., & Shaddad, M. H. 2010, *Meteoritics and Planetary Science*, 45, 1836  
 Horstmann, M., Bischoff, A., Pack, A., & Laubenstein, M. 2010, *Meteoritics and Planetary Science*, 45, 1657  
 Ida, S., Guillot, T., & Morbidelli, A. 2008, *ApJ*, 686, 1292  
 Ivanov, A. V., Ulyanov, A. A., Skripnic, A. Y., & Konokona, N. N. 1984, *Lunar and Planetary Institute Science Conference Abstracts*, 15, 393  
 Ivezić, Ž., Jurić, M., Lupton, R.H., Tabachnik, S., & Quinn, T. 2002, in *Survey and Other Telescope Technologies and Discoveries*, J.A. Tyson, S. Wolff, Editors, *Proceedings of SPIE Vol. 4836*  
 Jenniskens, P., Shaddad, M. H., Numan, D., Elsir, S., Kudoda, A. M., Zolensky, M. E., Le, L., Robinson, G. A., Friedrich, J. M., Rumble, D., Steele, A., Chesley, S. R., Fitzsimmons, A., Duddy, S., Hsieh, H. H., Ramsay, G., Brown, P. G., Edwards, W. N., Tagliaferri, E., Boslough M. B., Spalding, R. E., Dantowitz, R., Kozubal, M., Pravec, P., Borovicka, J., Charvat, J., Vaubaillon, J., Kuiper, J., Albers, J., Bishop, J. L., Mancinelli, R. L., Sandford, S. A., Milan, S. N.n Nuevo, M. & Worden S. P. 2009, *Nature*, 458, 485  
 Jenniskens, P., Vaubaillon, J., Binzel, R. P., DeMeo, F. E., Nesvorný, D., Bottke, W. F., Fitzsimmons, A., Hiroi, T., Marchis, F., Bishop, J. L., Vernazza, P., Zolensky, M. E., Herrin, J. S., Welten, K. C., Meier, M. M. M., & Shaddad M. H. 2010, *Meteoritics and Planetary Science*, 45, 1590  
 Johansen A., Oishi J. S., MacLow M. M., Klahr H., Henning T., Youdin A., 2007, *Nature*, 448, 1022  
 Johansen, A., Youdin, A., & Mac Low, M.-M. 2009, *ApJ Letters*, 704, L75  
 Jordi, C., Gebran, M., Carrasco, J. M., de Bruijne, J., Voss, H., Fabricius, C., Knude, J., Vallenari, A., Kohley, R., & Mora, A. 2010, *A&A*, 523, A48

- Kenyon, S. J., & Bromley, B. C. 2004, *AJ*, 127, 513
- Marchi, S., Paolicchi, P., Lazzarin, M., & Magrin, S. 2006, *AJ*, 131, 1138
- Meibom, A., & Clark, B. E. 1999, *Meteoritics and Planetary Science*, 34, 7
- Melosh, H. J. 1989, *Impact Cratering: A Geologic Process*, Oxford University Press
- Michel, O., Bendjoya, P., & Rojo Guerra, P. 2005, *Traitement du signal et des images*. UCL Presses Universitaires, de Louvain, p. 257
- Mignard, F., Cellino, A., Muinonen, K., Tanga, P., Delbò, M., Dell'Oro, A., Granvik, M., Hestroffer, D., Mouret, S., Thuillot, W., & Virtanen, J. 2007, *Earth Moon and Planets*, 101, 97
- Morbidelli, A., & Nesvorný, D. 1999, *Icarus*, 139, 295
- Morbidelli, A., Bottke, W. F., Jr., Froeschlé, C., & Michel, P. 2002, *Asteroids III*, 409
- Morbidelli, A., Bottke, W. F., Nesvorný, D., & Levison, H. F. 2009, *Icarus*, 204, 558
- Nesvorný, D., Vokrouhlický, D., Morbidelli, A., & Bottke, W. F. 2009, *Icarus*, 200, 698
- Nesvorný, D. 2010, *Nesvorný HCM Asteroid Families V1.0. EAR-A-VARGBDET-5-NESVORNYFAM-V1.0. NASA Planetary Data System*
- Paolicchi, P., Marchi, S., Nesvorný, D., Magrin, S., & Lazzarin, M. 2007, *A&A*, 464, 1139
- Parker, A., Ivezić, Ž., Jurić, M., Lupton, R., Sekora, M. D., & Kowalski, A. 2008, *Icarus*, 198, 138
- Shaddad M. H., Jenniskens, P., Numan, D., Kudoda, A. M., Elsir, S., Riyad I. F., Ali, A. E., Alameen, M., Alameen, N. M., Eid, O., Osman, A. T., Abubaker, M. I., Yousif, M., Chesley, S. R., Chodas, P. W., Albers, J., Edwards, W. N., Brown, P. G., Kuiper, J., & Friedrich, J. M. 2010, *Meteoritics and Planetary Science*, 45, 1557
- Singletary, S. J., & Grove, T. L. 2003, *Meteoritics and Planetary Science*, 38, 95
- Spurný, P., Haloda J., & Borovicka J., 2012, *LPI Contributions (Asteroids, Comets, Meteors Meeting)*
- Tholen, D. J. 1984, Ph.D. Thesis, Arizona University
- Vernazza, P., Binzel, R. P., Thomas, C. A., DeMeo, F. E., Bus, S. J., Rivkin, A. S., & Tokunaga, A. T. 2008, *Nature*, 454, 858
- Vokrouhlický, D., Brož, M., Bottke, W. F., Nesvorný, D., & Morbidelli, A. 2006, *Icarus*, 182, 118
- Walsh, K. J., Delbo, M., Muller, M., Binzel, R. P., & De Meo, F., 2012, *ApJ*, 748, 104
- Weidenschilling, S. J. 2011, *Icarus*, 214, 671
- Welten, K. C. et al. 2010, *Meteoritics and Planetary Science*, 45, 1728
- Wetherill, G. W. 1967, *Journal of Geophysical Research*, 72, 2429
- Wetherill, G. W., & Stewart, G. R. 1993, *Icarus*, 106, 190